Chem Rev Lett 6 (2023) 308-326

Research Article

Chemical Review and Letters
journal homepage: www.chemrevlett.com
ISSN (online): 2645-4947 (print) 2676-7279

A comprehensive investigation into the effect of substitution on electronic structure, charge transfer, resonance, and strength of hydrogen bond in 3–amino-propene thial and its analogous: A DFT calculation

Maliheh Javdani Zamani Sagheb[1,*], Leila Hokmabady[1], Azadeh Khanmohammadi[1]

[1]*Department of Chemistry, Payame Noor University, P.O. Box 19395-4697 Tehran, Iran*

ARTICLE INFO

Article history:
Received 13 September 2023
Received in revised form 15 October 2023
Accepted 19 October 2023
Available online 26 October 2023

Keywords:
3-amino-propene thial
2-hydrazineylidene-ethane thial
intramolecular hydrogen bonding
AIM
NMR

ABSTRACT

In this study, the effect of substitution (CH_2OCH_3, Cl, F, $NHCH_3$, NO_2, OH, Ph, $PhOCH_3$, and SH) on the hydrogen bonding energies of N-H···S intramolecular bridges in the 3-amino-propene thial and its analogous compound, 2-hydrazineylidene-ethane thial, is examined using density functional theory (DFT). The outcomes reveal that the compounds containing the Ph and F substitutions possess the strongest and weakest hydrogen bonds. In other words, the electron-donating substitutions strengthen the hydrogen bond, whereas electron-withdrawing ones weaken it. The hydrogen bonding formation can cause elongation of the N-H bond and shortening of the H···S distance. The findings derived from atoms in molecules (AIM) calculations show characteristics of closed-shell interactions and also the electrostatic nature of the H···S bonding. Moreover, the natural bond orbital (NBO) approach is employed to compute the interaction between the LP_S and the σ^*_{N-H}, which reveals that the largest interaction is related to the strongest hydrogen bond. Finally, to investigate the effect of the environment on the strength of hydrogen bonding, the calculations are conducted in two solvents, namely water and CCl_4. The outcomes indicate that hydrogen bonding strength is lower in the solution as compared to the gas phase.

1. Introduction

The comprehension of the configuration and characteristics of hydrogen bonding (HB) is of great significance owing to its pervasiveness in both inorganic and organic compounds, as well as biomolecules, inclusive of hormones, coenzymes, and proteins [1-3]. HB plays a pivotal role in biological procedures, chemical reactions, and the generation of crystalline structures, potentially leading to structural distortions in a plethora of molecules, spanning from water to DNA [4]. The HB is commonly known as an electrostatic dipole-dipole interaction, but it also exhibits characteristics of covalent bonding. It is directional, robust, and can generate interatomic distances shorter than the sum of van der Waals radii [5]. These properties are particularly evident when acceptors bind hydrogens from more electronegative donors [6]. The formation of intramolecular HB significantly affects the molecular structure and modulates the properties of molecules and numerous chemical processes.

The theoretical and experimental interest in this type of HBs has increased over many years [7-16]. The HB has significant impacts on the mechanical, thermal, and electrical properties of materials, as indicated in [17]. A thorough understanding of the fundamental nature of HB can aid in the design of materials with customized properties for various applications. For instance, polymers with strong HB can function as adhesives or coatings, while those with weak HB can serve as

∗ Corresponding author.; e-mail: malihehjavdani2023@gmail.com
https://doi.org/ 10.22034/CRL.2023.416216.1248

insulators [18]. Moreover, HB can greatly affect material processing, such as solubility and viscosity, thereby improving the efficiency and effectiveness of different manufacturing processes [19].

The HB also plays a vital role in the development of novel materials for energy storage [20, 21]. Specifically, the HB can stabilize polymers and enhance their charge transport properties, thus enabling the creation of innovative materials for energy storage purposes, e.g., batteries and supercapacitors. Moreover, HB can be utilized in the development of new materials for drug delivery [22, 23]. For example, the HB can be employed to fabricate self-assembling materials that can encapsulate drugs and release them in a controlled manner. By comprehending the nature of HB, researchers can design highly effective materials that can deliver drugs to specific targets in the body.

3-Amino-propene thial is a chemical compound that has been studied for its potential medical and antibacterial properties [24]. Specifically, it has been shown to have revascularizing effects in the pancreas and is being studied as a radioprotectant [25]. Additionally, some 1,3-Bis(aryloxy)propan-2-amines, which are structurally similar to 3-amino-propene thial, have been found to inhibit the growth of Gram-positive bacteria in the low micromolar range [24]. Understanding the chemical properties and behavior of this compound could also provide insight into its potential uses in other fields. For example, studying the reactivity and stability of similar flavor compounds has led to the discovery of important secondary products [26].

Due to the fundamental significance of intramolecular HBs in structural, chemical, and biological processes, a thorough investigation of the substitution effects (H, CH_2OCH_3, Cl, F, $NHCH_3$, NO_2, OH, Ph, $PhOCH_3$, and SH) on the characteristics of HB in 3-amino-propene thiol (APT) and 2-hydrazineylidene-ethane thial (HET) has been conducted in both gas phase and solution (CCl_4 and water). In these compounds, the HB strength has been assessed by replacing the carbon atom (APT) with nitrogen (HET) within the structure (refer to Scheme 1). An asymmetric N-H···S intramolecular HB is present, which is significantly influenced by π-electron delocalization, thereby affecting the HB geometry and strength.

The aim of this study is to explore various calculations encompassing energetic, electronic, geometric, spectroscopic, and topological parameters of the aforementioned molecules. Physical properties such as dipole moment, chemical potential, and chemical hardness have been evaluated to achieve this objective. Additionally, aromaticity indices, vibrational frequencies, charge transfer analysis, and ^{1}HNMR chemical shifts have been performed to gain an understanding of the electronic structure of these compounds.

The findings of this study can potentially be used in the development of novel molecules with specific hydrogen bonding interactions. By selectively incorporating substitutions that reinforce or weaken the H···S contact, researchers may be able to optimize the properties of the molecule for a specific application. The implications of these findings could be significant in the field of drug design, where understanding the strength and nature of intramolecular interactions is crucial in determining the efficacy and stability of drugs. Here are some examples of relevant drugs and their structures, which can help readers understand the potential applications and significance of the study:

Anticancer drugs: This investigation can have implications for the design of new anticancer drugs. For example, the structure of the anticancer drug cisplatin, which contains a platinum atom coordinated with two ammonia ligands and two chloride ligands, can be included to illustrate the relevance of the research.

Antibiotics: The research can also be relevant to the design of new antibiotics. For example, the structure of the antibiotic penicillin, which contains a beta-lactam ring and a thiazolidine ring, can be included to demonstrate the potential applications of the study.

Antiviral drugs: This study can also be relevant to the design of new antiviral drugs. For example, the structure of the antiviral drug oseltamivir, which contains a guanidine group and a cyclohexene ring, can be included to illustrate the potential applications of the research.

Neurotransmitters: The research can also have implications for the design of new drugs that target neurotransmitter receptors. For example, the structure of the neurotransmitter acetylcholine, which contains a quaternary ammonium group and an acetyl group, can be included to demonstrate the relevance of the study.

2. Computational details

All computations are performed using the quantum chemistry package Gaussian 09 [27]. The optimized structural parameters of the species and their derivatives are obtained at the B3LYP computational level employing the 6-311++G(d,p) basis set. Frequency computations are conducted to validate the characteristics of the stationary points and to provide a description for the correction of zero-point vibrational energy (ZPVE). The effect of the solvent is assessed in two solutions consisting of CCl_4 and water, utilizing the

polarizable continuum model (PCM) [28]. To identify the crucial points (bond critical points, BCPs, and ring critical points, RCPs) and analyze them in terms of electron density (ρ), its Laplacian ($\nabla^2\rho$), the total electron energy density at the critical point (H_C), and its two components, including the potential electron energy density (V_C) and the kinetic electron energy density (G_C), the Quantum Theory of "Atoms in Molecules" (QTAIM) of Bader [29, 30] is applied. The AIM2000 program is employed for the AIM calculations [31]. The Laplacian and the energetic characteristics of the critical point have a well-established relationship [29] as follows:

$$1/4\ (\nabla^2\rho_C) = 2G_C + V_C \text{ and } H_C = G_C + V_C \quad (1)$$

The estimation of HB energy is achieved by utilizing the Espinosa method [32], which involves analyzing the properties of bond critical points. In order to evaluate the nature of intramolecular interactions, the natural bond orbital (NBO) [33] analysis is employed. Additionally, the calculation of absolute NMR shielding values [34] is carried out using the Gauge-Independent Atomic Orbital (GIAO) method [35]. To measure the aromaticity of the formed rings, several well-established indices of aromaticity are utilized. One such measure is the harmonic oscillator model of aromaticity (HOMA) index, which is a structure-based indicator defined by Kruszewski and Krygowski [36-38] as

$$\mathrm{HOMA} = 1 - \frac{\propto}{n}\sum_{i=1}^{n}\left(R_{opt} - R_i\right)^2 \quad (2)$$

The quantity "n" represents the number of bonds taken into consideration in the present context, and the symbol "α" denotes an empirical constant. "R_{opt}" indicates the optimal bond length value for ideally aromatic systems, whereas "R_i" represents a running bond length. Ideally, aromatic systems exhibit an HOMA value of 1, while nonaromatic models have a HOMA value of 0. Additionally, the Nucleus Independent Chemical Shift (NICS) [39] serves as an alternative aromaticity index, which is the most popular magnetic factor of aromaticity. Poater et al. also proposed a para-delocalization index (PDI), which calculates the average of the delocalization indices of para-related atoms in a six-membered ring [40] as

$$\mathrm{PDI} = \frac{\delta(1,4) + \delta(2,5) + \delta(3,6)}{3} \quad (3)$$

The primary limitation of PDI entails its applicability only to six-membered rings. However, this inadequacy is effectively resolved through the implementation of average two-center indices (ATI) [41] as follows:

$$\mathrm{ATI} = \frac{1}{n}\sum_{A-B}^{n}\delta(A,B) \quad (4)$$

where the summation runs over all adjacent pairs of atoms surrounding the n-membered ring and the delocalization index δ(A, B) is derived from the AIM theory. Another criterion for determining aromaticity is the aromatic fluctuation index (FLU) [42]. This index characterizes the fluctuation of the electronic charge between adjacent atoms within a given ring and is based on a comparison with the cyclic electron delocalization of a typical aromatic molecule. In this study, we compute the R_{opt}, α, and δ_{ref} parameters for the HOMA and FLU indices at the B3LYP/6-311++G(d,p) level of theory (for CS, CC, CN, and NN bonds: $R_{opt,CS}$ = 1.689 Å, $R_{opt,CC}$ = 1.399 Å, $R_{opt,CN}$ = 1.333 Å, $R_{opt,NN}$ = 1.286 Å, α_{CS} = 74.563, α_{CC} = 80.661, α_{CN} = 91.476, α_{NN} = 75.696, $\delta_{ref,CS}$ = 4.626, $\delta_{ref,CC}$ = 1.385, $\delta_{ref,CN}$ = 1.32, and $\delta_{ref,NN}$ = 1.526). Finally, the selected compounds and their derivatives undergo molecular orbital calculations, including the highest occupied molecular orbital (HOMO) and lowest unoccupied molecular orbital (LUMO).

3. Results and discussion

3.1. Molecular geometry and energetic analysis

The present study illustrates the structural difference between APT and HET compounds based on the position of substitutions (R) on the ring, where R includes H, CH_2OCH_3, Cl, F, $NHCH_3$, NO_2, OH, Ph, $PhOCH_3$, and SH, as depicted in Scheme 1. These compounds are fully optimized at the B3LYP/6-311++G(d,p) level of theory and the outcomes are reported in Table 1. It is a well-established fact that the geometrical parameters of HB systems (X-H···Y) reflect the bond strength [43]. Typically, a stronger HB is associated with a shorter H···Y distance. For the N-H···S intramolecular bridges, this leads to the elongation of the N-H bond and the reduction of the H···S distance. Analysis of geometrical parameters reveals that the H···S distances in the chelated rings of APT and HET are in the ranges of 2.210–2.287 Å and 2.170–2.262 Å, respectively, indicating lower H···S values in the HET group compared to APT. This implies that the HB strength in the HET compound and its derivatives is higher than that in APT. In other words, the replacement of the nitrogen atom instead of carbon in

the structure leads to an increase in the HB strength, as shown in Scheme 1.

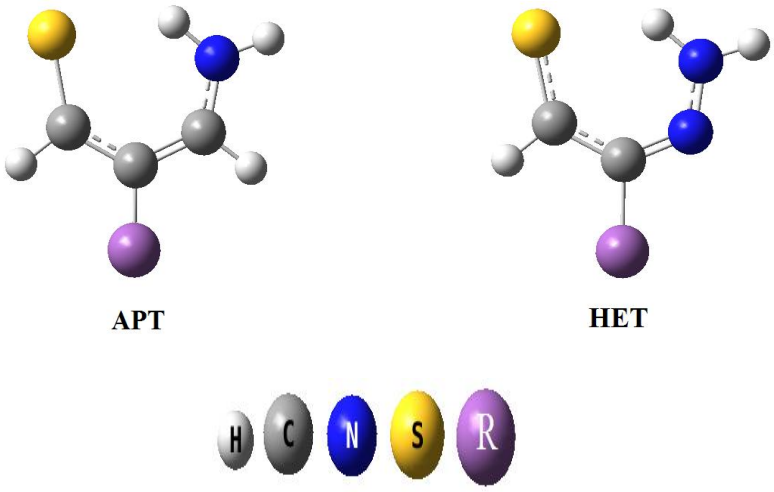

Scheme 1. The optimized structures of APT and HET, R = H, CH_2OCH_3, Cl, F, $NHCH_3$, NO_2, OH, Ph, $PhOCH_3$, and SH.

Table 1. HB geometrical parameters (distances (d), in Å and angles (θ), in °), HB energies (E^*_{HB}, in kJ mol^{-1}) and stretching frequencies (υ, in cm^{-1}) of APT, HET and their derivatives.

	APT					**HET**				
R	d_{N-H}	$d_{H\cdots S}$	θ_{SHN}	E^*_{HB}	υ_{N-H}	d_{N-H}	$d_{H\cdots S}$	θ_{SHN}	E^*_{HB}	υ_{N-H}
H	1.024	2.262	135.5	-25.38	3309.0	1.026	2.214	136.0	-28.90	3263.1
CH_2OCH_3	1.025	2.230	135.9	-27.78	3291.9	1.026	2.196	136.0	-30.39	3267.9
Cl	1.024	2.251	135.0	-26.28	3315.8	1.024	2.224	134.2	-28.31	3302.4
F	1.023	2.287	134.6	-23.80	3336.8	1.022	2.262	133.6	-25.51	3334.0
$NHCH_3$	1.024	2.238	135.6	-27.21	3304.3	1.022	2.215	135.0	-28.78	3320.2
NO_2	1.027	2.235	135.8	-27.61	3267.5	1.028	2.211	134.8	-29.62	3240.9
OH	1.023	2.258	135.1	-25.75	3322.9	1.023	2.215	134.8	-28.89	3315.7
Ph	1.026	2.210	136.2	-29.43	3278.3	1.027	2.170	136.3	-32.83	3248.1
$PhOCH_3$	1.025	2.211	136.2	-29.34	3279.2	1.026	2.170	136.3	-32.79	3252.9
SH	1.025	2.231	135.7	-27.76	3296.2	1.026	2.189	135.7	-31.15	3258.7

The results obtained from the study reveal that the Ph and F substitutions have the minimum and maximum H···S contacts in the APT and HET groups, respectively. It can be inferred that the compounds containing the Ph substitution possess the strongest HBs, while those with the F substitution have the weakest HBs. Additionally,

upon evaluating all substitutions, it is observed that the H···S distance for electron-donating substitutions, such as Ph and $PhOCH_3$, is shorter than that of electron-withdrawing substitutions, such as F, Cl, and OH. This indicates that the electron-donating substitutions strengthen the HB, while the electron-withdrawing ones weaken it. In the APT group, the H···S distance decreases compared to that of the parent molecule (H substitution) except for the F substitution. This suggests that the HB strength in the APT molecule is relatively weaker than its derivatives. The NHS bond angle may also explain the strength of HBs, where a closer bond angle to 180° corresponds to a stronger HB. Table 1 indicates that the maximum NHS bond angle in groups of APT and HET is associated with the shortest H···S contact.

This study assesses the intramolecular HB energies (E^*_{HB}) using the Espinosa method [32]. The estimation of E^*_{HB} may be derived from the features of bond critical points. The correlation between E^*_{HB} and potential energy density at the critical point, $V(r_{CP})$, corresponding to H···S contact, is expressed as $E^*_{HB} = 1/2\ V(r_{CP})$. The E^*_{HB} values are tabulated in Table 1. Based on the outcomes, the studied substitutions can be divided into two groups as follows:

1. The substitutions that increase the HB strength compared to the parent compound are as follows:

In the APT group: Ph > $PhOCH_3$ > CH_2OCH_3 > SH > NO_2 > $NHCH_3$ > Cl > OH
In the HET group: Ph > $PhOCH_3$ > SH > CH_2OCH_3 > NO_2

2. The substitutions that decrease the HB strength compared to the parent molecule are as follows:

In the APT group: F
In the HET group: OH > $NHCH_3$ > Cl > F

Linear relationships exist between E^*_{HB} and the H···S distances ($d_{H\cdots S}$) with correlation coefficients equal to 0.998 and 0.996 for the APT and HET groups, respectively (see Scheme 2). As shown in the Scheme, the HB strength increases as the H···S distance decreases. Conversely, an opposite pattern is observed for the N-H distances, demonstrating that HB strength enhances as the N-H bond length increases.

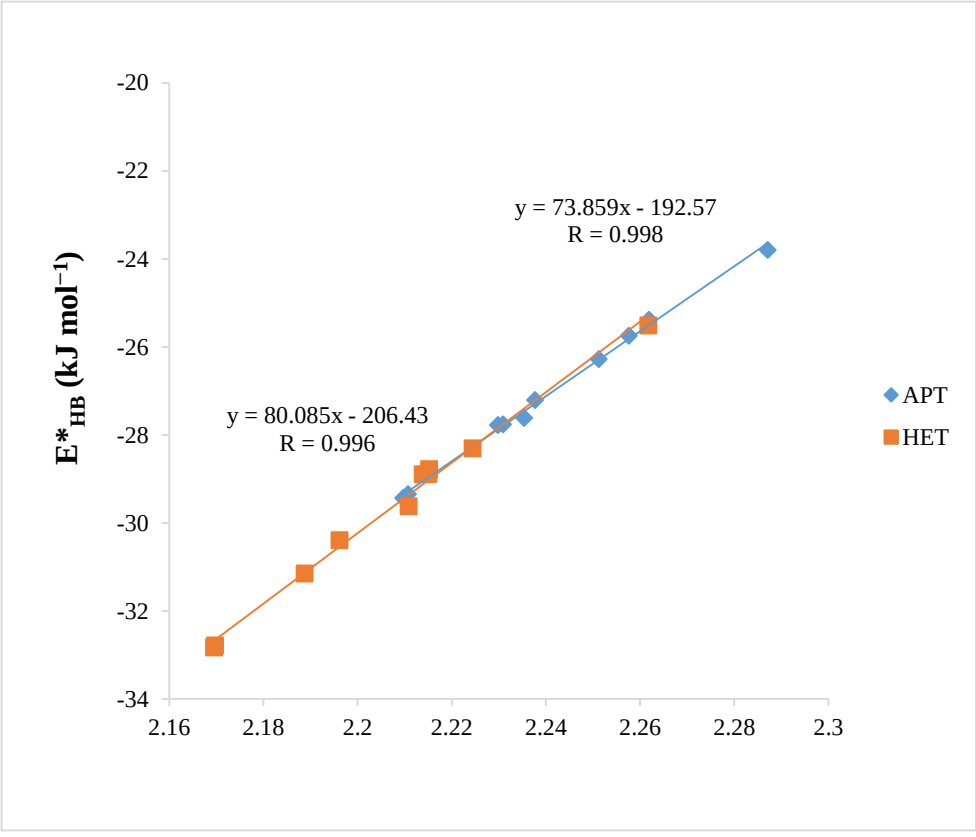

Scheme 2. The relationship between the E^*_{HB} and $d_{H\ldots S}$.

3.2. Vibrational frequencies

In order to perform a more comprehensive investigation of the effectiveness of HBs, the vibrational frequencies of all compounds have been calculated and recorded in Table 1. The formation of HB results in a decrease in the frequency of the N-H stretching mode as observed. This study examines molecules that exhibit both red and blue shifts. Notably, the N-H stretching frequencies for the F substitution of APT and HET displays blue shifts of approximately 28 and 80 cm^{-1} relative to the parent molecule, whereas those for the Ph substitution exhibit red shifts of nearly 31 and 15 cm^{-1}, respectively. Stronger HBs result in greater red shifts of stretching frequencies, as the proton-donor bond lengthens due to HB formation.

The results of our investigation demonstrate that in the majority of instances, the electron-withdrawing substituents (F and Cl) exhibit the greatest stretching frequencies, while electron-donating ones (Ph and $PhOCH_3$) display the smallest values (see Table 1). Among all compounds examined, the F substitution yields the highest stretching frequency, while the Ph substitution presents the lowest value, denoting that the strongest HB corresponds to the smallest stretching frequency and vice versa (apart from NO_2). Remarkably, exceptional linear relationships exist between υ_{N-H} and d_{N-H}, with correlation coefficients (R) amounting to 0.946 and 0.981 in APT and HET groups, respectively, and an equation as follows:

υ_{N-H} = -16275 (-15876) d_{N-H} + 19975 (19554)

The aforementioned finding implies that the reinforcement of the HB results in a rise in the N-H distance, which is accompanied by a decrease in its stretching frequency.

3.3. AIM analysis

Bader's theory represents a valuable instrument in elucidating the interaction between atoms [29]. The bond critical points (BCPs) possess various properties, among which the electron density (ρ_{BCP}) and its Laplacian ($\nabla^2\rho_{BCP}$) provide information on the nature of the interaction. Two general classes are considered for atomic interactions. Specifically, when $\nabla^2\rho_{BCP} < 0$ and ρ_{BCP} assumes a large value, it indicates the concentration of electronic charge within the internuclear region, which is suggestive of shared-shell interactions (covalent bonds). Conversely, when $\nabla^2\rho_{BCP} > 0$ and ρ_{BCP} assumes a small value, the electronic charge within the internuclear region is depleted, and such interactions are characteristic of closed-shell systems, such as ionic, van der Waals, and HB. Koch and Popelier have posited that the electron density value of the hydrogen bond critical point (ρ_{HB}) spans the range of 0.002-0.040 a.u. [44].

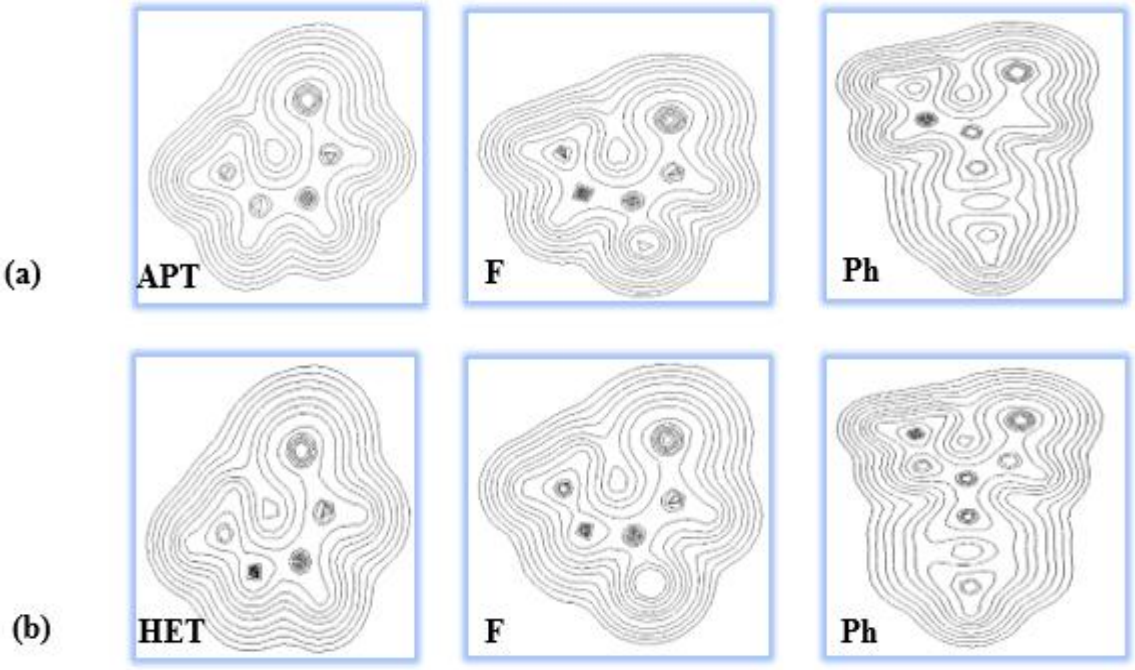

Scheme 3. The contour map representing (a) APT and (b) HET molecules, along with their F and Ph derivatives.

Table 2. The selected topological properties of electron density (in a.u.) obtained by AIM analysis.

	APT						HET					
	$\rho_{H\cdots S}$	$\nabla^2\rho_{H\cdots S}$	ρ_{RCP}	$\nabla^2\rho_{RCP}$	H_C	$-G_C/V_C$	$\rho_{H\cdots S}$	$\nabla^2\rho_{H\cdots S}$	ρ_{RCP}	$\nabla^2\rho_{RCP}$	H_C	$-G_C/V_C$
H	0.0275	0.0596	0.0119	0.0691	0.0040	1.4277	0.0300	0.0646	0.0133	0.0779	0.0043	1.4018
CH_2OCH_3	0.0293	0.0619	0.0123	0.0718	0.0041	1.4220	0.0311	0.0663	0.0136	0.0794	0.0044	1.3983
Cl	0.0281	0.0610	0.0121	0.0695	0.0040	1.4204	0.0294	0.0653	0.0132	0.0759	0.0042	1.3965
F	0.0262	0.0585	0.0117	0.0666	0.0038	1.4255	0.0273	0.0628	0.0129	0.0727	0.0040	1.3979
$NHCH_3$	0.0288	0.0618	0.0121	0.0706	0.0041	1.4251	0.0297	0.0663	0.0132	0.0768	0.0043	1.4012
NO_2	0.0293	0.0608	0.0120	0.0713	0.0041	1.4164	0.0306	0.0644	0.0136	0.0779	0.0043	1.3895
OH	0.0277	0.0606	0.0119	0.0690	0.0040	1.4266	0.0298	0.0665	0.0134	0.0769	0.0043	1.3966
Ph	0.0305	0.0633	0.0125	0.0733	0.0042	1.4200	0.0328	0.0682	0.0139	0.0816	0.0045	1.3940
$PhOCH_3$	0.0305	0.0633	0.0125	0.0732	0.0042	1.4202	0.0328	0.0683	0.0139	0.0816	0.0045	1.3940
SH	0.0293	0.0621	0.0123	0.0712	0.0041	1.4199	0.0316	0.0668	0.0136	0.0796	0.0044	1.3965

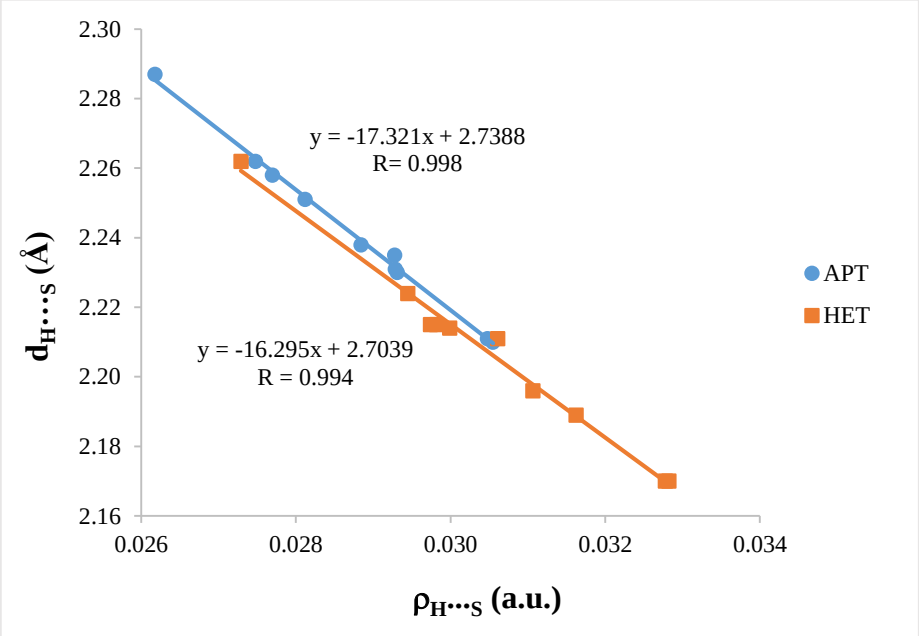

Scheme 4. The relationship between the $d_{H\ldots S}$ and $\rho_{H\ldots S}$.

The topological parameters of the compounds under investigation are presented in Table 2. As illustrated in the aforementioned table, the H···S bonds exhibit low ρ values (ranging from 0.0262 to 0.0305 for APT and 0.0273 to 0.0328 for HET) and positive $\nabla^2\rho$ values (ranging from 0.0585 to 0.0633 for APT and 0.0628 to 0.0683 for HET). These attributes are characteristic of closed-shell interactions and indicate the electrostatic

nature of the H···S bonds. Furthermore, within the APT and HET groups, the $\rho_{H\cdots S}$ values for the Ph and $PhOCH_3$ substitutions are notably higher than the others, providing further evidence for the existence of stronger HBs (refer to Table 2). It is noteworthy that the replacement of C with N within the structure induces greater changes in the topological parameters of the compounds. The contour maps of Laplacian of electron density ($\nabla^2\rho$) for the APT and HET molecules, along with their F and Ph derivatives, are depicted in Scheme 3.

The analyzed species exhibit exceptional correlations between their topological and geometrical parameters. Linear relationships between the distance and electron density of H···S contacts are established with correlation coefficients greater than 0.99, as illustrated in Scheme 4. This implies that the $\rho_{H\cdots S}$ values play a crucial role in assessing the strength of HBs in the investigated systems. The ring critical point (RCP) represents a location where the electron density is at its lowest point on the ring surface, while simultaneously reaching its highest on the ring line, as cited in reference [45]. Notably, substituted systems display good correlations between the E^*_{HB} and the ρ_{RCP}, with correlation coefficients of 0.957 and 0.978 for APT and HET groups, respectively (refer to Scheme 5). Therefore, it is evident that RCP properties can serve as a reliable measure of HB strength [46].

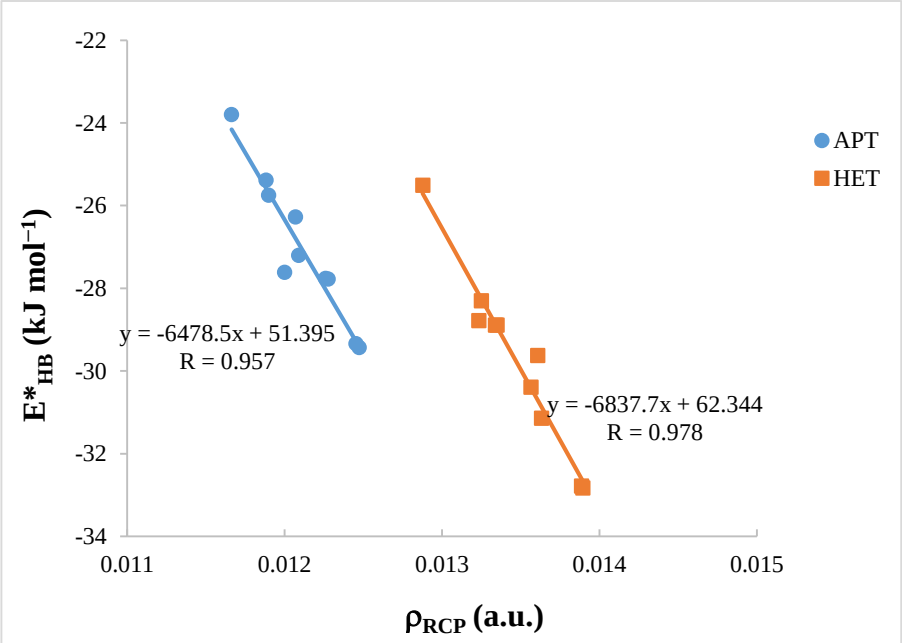

Scheme 5. The relationship between the E^*_{HB} and ρ_{RCP}.

The $-G_C/V_C$ ratio also acts as a criterion for determining the nature of HBs [47, 48]: the value of $-G_C/V_C \geq 1$ indicates a non-covalent HB, while $0.5 < -G_C/V_C < 1$ suggests a partially covalent HB. Based on the calculated electron density properties of the studied species, H···S contacts exhibit positive H_C values and $-G_C/V_C > 1$, as depicted in Table 2. These findings confirm that the HBs within the studied systems are non-covalent.

3.4. NBO analysis

The analysis of NBO [33] serves as a useful foundation for exploring molecular structures with regard to charge transfer or conjugative interactions. In the context of NBO analysis for HB systems, the transfer of charge between the lone pairs of the proton acceptor and the antibonding of the proton donor is of utmost significance. Table 3 presents the occupation numbers of sulfur lone pairs (LP_S) and $\sigma^*_{N\text{-}H}$ antibonding, as well as second-order perturbation energies ($E^{(2)}$), which correspond to the charge transfer between LP_S and $\sigma^*_{N\text{-}H}$ ($LP_S \rightarrow \sigma^*_{N\text{-}H}$). In this case, the HB leads to an increase in the occupancy of the $\sigma^*_{N\text{-}H}$ antibonding orbital, thereby resulting in a longer and weaker N-H bond. In certain instances, the alteration in the occupation numbers of LP_S and $\sigma^*_{N\text{-}H}$ aligns with the energy of charge transfer and the HB formation energy.

Table 3. The NBO analysis of the compounds including the second-order perturbation energy ($E^{(2)}$, in kcal mol^{-1}) and occupation numbers of LP_S and σ^*_{N-H}.

	APT			HET		
R	$E^{(2)}$	LP_S	σ^*_{N-H}	$E^{(2)}$	LP_S	σ^*_{N-H}
H	14.01	1.882	0.061	16.15	1.879	0.077
CH_2OCH_3	15.53	1.877	0.065	16.95	1.879	0.078
Cl	14.09	1.875	0.061	14.72	1.875	0.072
F	12.61	1.882	0.056	12.98	1.883	0.065
$NHCH_3$	14.98	1.879	0.063	15.00	1.883	0.071
NO_2	15.65	1.876	0.068	16.57	1.877	0.079
OH	13.82	1.879	0.059	15.01	1.878	0.071
Ph	16.58	1.875	0.068	18.42	1.875	0.082
$PhOCH_3$	16.51	1.875	0.068	18.32	1.876	0.082
SH	15.30	1.875	0.065	17.16	1.873	0.080

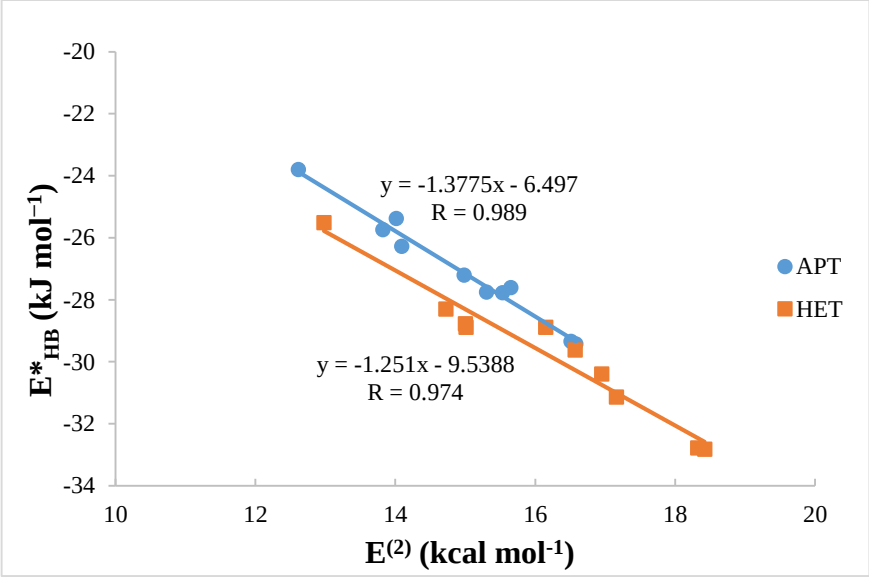

Scheme 6. The relationship between the E^*_{HB} and $E^{(2)}$.

Our research findings, as depicted in Table 3, demonstrate that the highest and lowest values of $E^{(2)}$ are attributed to the Ph and F substitutions, respectively. It is evident that the most substantial interaction is related to the strongest HB. The replacement of C with N atom in the molecular structure elicits an upsurge increase in the $E^{(2)}$ values of the HET group and its derivatives. Favorable associations can be drawn between the $E^{(2)}$ and E^*_{HB} values. The corresponding correlation coefficients for the APT and HET compounds and their derivatives

stand at 0.989 and 0.974, respectively (refer to Scheme 6). This indicates that the characteristics of the charge transfer between the lone pairs of proton acceptor and antibonding of proton donor could be exceptionally useful in evaluating the strength of the HB.

The outcomes of computational analyses further demonstrate that the $E^{(2)}$ values display a substantial correlation with other geometrical and topological parameters. To illustrate, the linear correlation coefficients of $E^{(2)}$ dependence on $d_{H\cdots S}$ and $\rho_{H\cdots S}$ are noted to be greater than 0.9 for both the APT and HET groups.

3.5. NMR analysis

The ^{1}HNMR chemical shift (δ^H) is a valuable tool for comprehending the electronic structure of molecules. The increase in strength of HB elicits a change in the ^{1}H chemical shift towards down fields. Examination of Table 4 reveals that the highest chemical shift values in the APT and HET groups are related to Ph substitution, which exhibits the strongest HBs. This observation illustrates that the formation of HB exerts a significant effect on the alteration of electronic charge distribution on hydrogen atom and its movement towards proton acceptor atom. Moreover, the lowest chemical shift is attributed to the F substitution (representing the compound with the weakest HB strength). A regression analysis has been conducted to assess the relationship between the ^{1}H chemical shifts and the E^*_{HB}, as depicted in Scheme 7.

Table 4. The chemical shifts (δ^H, in ppm) and spin-spin coupling constants ($^1J_{N\text{-}H}$ and $^1J_{H\cdots S}$, in Hz) of APT, HET and their derivatives.

	APT			HET		
R	δ^H	$^1J_{N\text{-}H}$	$^1J_{H\cdots S}$	δ^H	$^1J_{N\text{-}H}$	$^1J_{H\cdots S}$
H	11.89	70.45	4.41	14.42	71.69	5.91
CH_2OCH_3	12.22	70.09	4.54	14.43	71.84	5.84
Cl	11.70	70.74	4.55	13.68	73.16	5.69
F	10.92	71.24	4.48	12.74	74.08	5.52
$NHCH_3$	11.88	70.50	4.62	13.60	73.20	5.84
NO_2	12.25	69.82	4.18	14.44	72.33	5.60
OH	11.32	70.74	4.61	13.39	73.45	6.20
Ph	12.72	69.89	4.74	15.14	71.71	6.20
$PhOCH_3$	12.65	69.89	4.75	15.05	71.77	6.22
SH	12.14	70.06	4.53	14.63	71.64	5.94

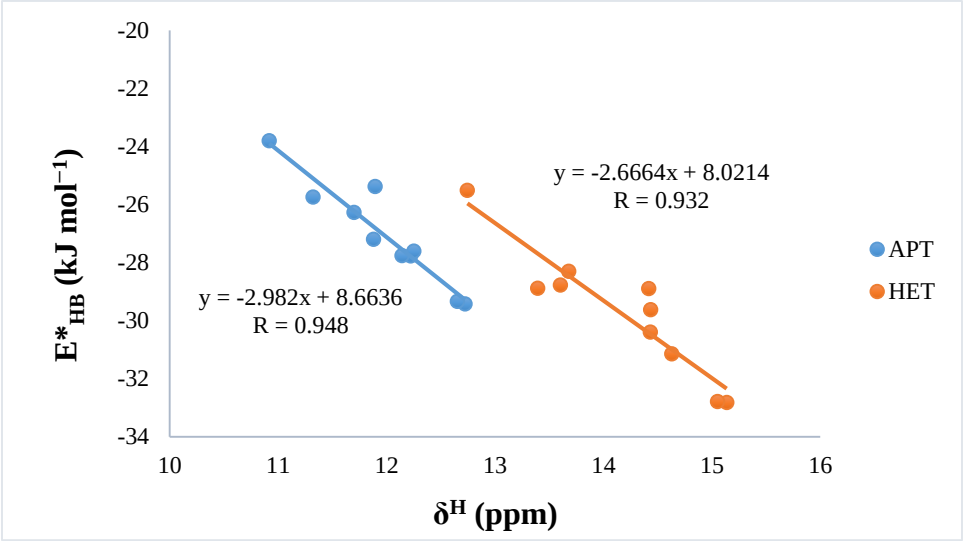

Scheme 7. The relationship between the E^*_{HB} and δ^H.

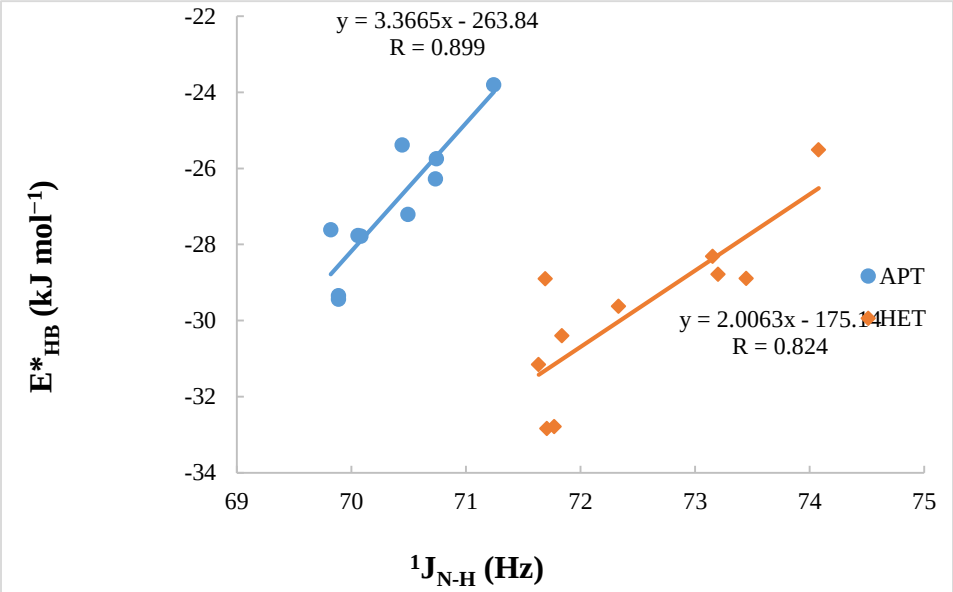

Scheme 8. The relationship between the E^*_{HB} and $^1J_{N-H}$.

Another aim of the present work is to provide a valuable and informative tool for representing the shift in electron density in regions where the formation of HB is expected. This has been achieved through the calculation of NMR spin Hamiltonian parameters, particularly the spin-spin coupling constants (J) for hydrogen nuclei involved in HB, with the resulting values being reported in Table 4. Notably, all $^1J_{N-H}$ coupling constants display positive values. Of particular interest, the highest value of $^1J_{N-H}$ observed in the APT and HET groups is associated with F substitution. As depicted in Scheme 8, the strength of HB exhibits a clear change relative to the $^1J_{N-H}$ coupling constant. A relatively good correlation between these two parameters is observed in both APT and HET compounds, as well as their derivatives. Moreover, Table 4 indicates that the replacement of C by N atoms enhances both δ^H and $^1J_{N-H}$ values in the considered compounds.

3.6. Resonance parameters

The findings of the aromaticity indices are presented in Table 5. As demonstrated in said table, the HOMA values exhibit proximity to the optimal aromaticity index (HOMA = 1). A higher HOMA index signifies greater delocalization of the π-system, thus indicating heightened aromaticity within the molecules. The results reveal that the HOMA values of APT and HET groups are within the ranges of 0.9716-0.9791 and 0.9391-0.9684, respectively. Based on these results, the APT group, characterized by high electron delocalization, becomes increasingly aromatic compared to the HET group. Consequently, the maximum HOMA index value in the APT group is attributed to R = OH. In the HET group, the substitution of H displays the highest degree of aromaticity. In certain cases, electron-withdrawing substitutions exhibit greater aromaticity than their electron-donating counterparts.

One of the most commonly employed magnetic indicators for detecting aromaticity is the nucleus-independent chemical shift (NICS), which is defined as the negative value of the absolute shielding computed at the center of the ring or at other significant points within the system [49]. Large negative values indicate the presence of aromaticity, while large positive values correspond to anti-aromaticity. Near-zero values, on the other hand, suggest non-aromaticity [50]. The computations for NICS are executed using Gaussian software at a distance of 1.5 Å above the chelate ring relative to the ring's center. Results are presented in Table 5. As evident from the Table, the highest aromaticity values in the APT and HET groups are associated with the CH_2OCH_3 substitution, whereas the lowest values are related to the H and $NHCH_3$ substitutions, respectively. As a more negative NICS value is indicative of a higher degree of aromaticity, it can be inferred from the findings that the system becomes more aromatic with the CH_2OCH_3 substitution.

Table 5. Calculated aromaticity indices related to the chelate ring of the examined structures.

	APT					**HET**				
R	HOMA	FLU	PDI	ATI	NICS	HOMA	FLU	PDI	ATI	NICS
H	0.9774	0.1736	0.0596	1.0625	-0.8695	0.9684	0.2526	0.0698	1.1024	-1.3175
CH_2OCH_3	0.9756	0.1719	0.0568	1.0474	-1.6310	0.9540	0.2510	0.0660	1.0879	-1.9761
Cl	0.9771	0.1679	0.0583	1.0538	-0.9821	0.9510	0.2441	0.0657	1.0965	-1.2860
F	0.9743	0.1661	0.0635	1.0532	-1.1506	0.9515	0.2392	0.0701	1.0879	-1.4062
$NHCH_3$	0.9716	0.1698	0.0601	1.0428	-1.0606	0.9391	0.2459	0.0699	1.0738	-0.9445
NO_2	0.9750	0.1574	0.0437	1.0551	-1.2039	0.9575	0.2409	0.0557	1.1003	-1.5315
OH	0.9791	0.1723	0.0644	1.0434	-1.1081	0.9570	0.2449	0.0762	1.0750	-1.4244
Ph	0.9748	0.1735	0.0580	1.0415	-1.4888	0.9508	0.2531	0.0674	1.0795	-1.0105
$PhOCH_3$	0.9748	0.1768	0.0588	1.0366	-1.6141	0.9497	0.2547	0.0682	1.0759	-1.1401
SH	0.9754	0.1695	0.0545	1.0527	-1.0808	0.9527	0.2487	0.0641	1.0981	-1.2379

Another index of aromaticity utilized for investigating chemical bonds is the aromatic fluctuation index (FLU). The FLU index measures the relative electronic deviation of a molecule compared to a reference molecule, and the closer the parameter value is to zero, the greater the degree of aromaticity in the ring. As indicated by Table 5, the NO_2 substitution possesses the lowest FLU index value of 0.1574 in the APT, suggesting the presence of greater aromaticity in this compound. Similarly, the F substitution exhibits the lowest value of this index in HET, implying that the maximum degree of aromaticity corresponds to the weakest HB. Based on a comparison of FLU electronic indices across the compounds, it can be inferred that the order of decreasing aromaticity is as follows: APT > HET.

The PDI, which is exclusively proposed for six-membered rings, is another index of aromaticity. However, due to its limited usage for these rings, the ATI parameter is employed to rectify this deficiency. Based on Table 5, the NO_2 substitution in the compounds of APT and HET corresponds to the lowest values of PDI, while OH substitution corresponds to the highest values. In both sets, the substituted compounds exhibit lower values of the ATI index compared to the parent molecule. The substituted $PhOCH_3$ in APT has the lowest value of this index at 1.0366, while the $NHCH_3$ substitution in the HET group has a numerical value of 1.0738.

3.7. Dependence between substituent constants and resonance parameters

The observed changes in this study can be attributed to the effect of R substitution on the electronic structure of the pseudo-ring of the HB. It is noteworthy that this effect manifests itself in two distinct ways: firstly, the mesomeric effect, whereby the substitution is positioned with regards to the pseudo-ring π-electrons; and secondly, the field/inductive effect, which is predominantly associated with the electronegativity of the group attached to the pseudo-ring.

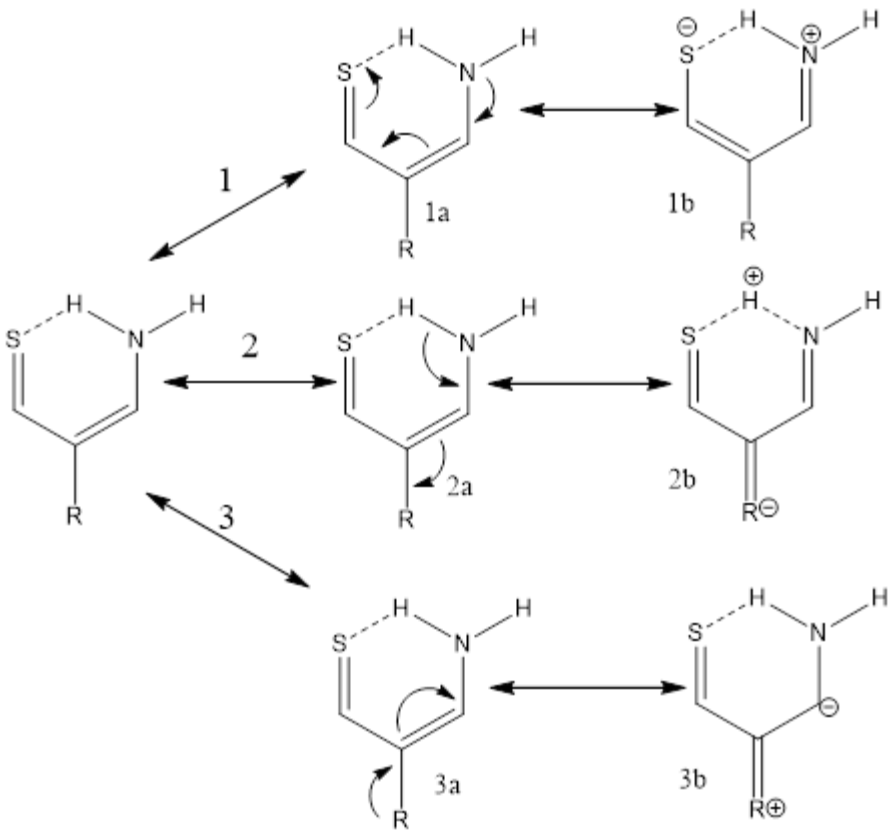

Scheme 9. Schematic representation of resonance (mesomeric) effect in APT systems substituted at position R.

Table 6. Substituent constants corresponding to the substituent's considered in this work.

R	σ^+	σ^-	F	R^+	R^-
H	0.00	0.00	0.00	0.00	0.00
CH_2OCH_3	-0.05	–*	0.13	-0.18	–*
Cl	0.11	0.19	0.42	-0.31	-0.23
F	-0.07	-0.03	0.45	-0.52	-0.48
$NHCH_3$	-1.81	–*	-0.03	-1.78	–*
NO_2	0.79	1.27	0.65	0.14	0.62
OH	-0.92	-0.37	0.33	-1.25	-0.70
Ph	-0.18	0.02	0.12	-0.30	-0.10
$PhOCH_3$	–*	–*	–*	–*	–*
SH	-0.03	–*	0.30	-0.33	–*

* Has not reported in the literature

Three mesomeric effects that cooperate or compete with each other demonstrate the three-way resonance in the APT system, as illustrated in Scheme 9. In the first case, the resonance effect occurs within the quasi-ring of the APT moiety (1a ↔1b). In this situation, the substitution does not impact the delocalization of π-electrons and the associated substitution retains its characteristic, which is similar to that of the unsubstituted APT molecule (R = H). This effect results in partial delocalization of π-bonds, thereby favoring the formation of HB.

The second case relates to the situation where the substituent appended to APT possesses electron-withdrawing characteristics and the entire system contributes to the delocalization of π-electrons (structures 2a and 2b). It can be hypothesized that induction and delocalization effects collaborate with each other. Indeed, for all systems with electron-withdrawing properties, there is a smaller N-H distance and a larger H···S distance, which suggests a weaker HB. In the third case, regarding electron-donating substitutions (structures 3a and 3b), the resonance effect in the HB is seriously restricted due to the presence of a negative

charge on the carbon atom. The HB energy calculations demonstrate that this effect enhances the HB strength in electron-donating substituents like Ph.

The substitution constants, namely σ^+, σ^-, F, R^+, and R^-, are crucial parameters that are empirically determined to explore the effect of substituent [51]. The corresponding values for the investigated substituents are comprehensively tabulated in Table 6. Certain correlations exist between the substitution constants and the aromaticity indices. Specifically, the PDI electronic index exhibits the most promising associations with σ^- and R^-. The correlation coefficients (R) are 0.976 and 0.950 for the APT group, and 0.972 and 0.922 for the HET group, respectively. Additionally, relatively favorable correlations are discovered between FLU and σ^-, as well as between FLU and F in the APT group. Furthermore, the HET group manifests significant linear relationships between the ATI index with σ^+ and R^+.

3.8. HOMO and LUMO analysis

The HOMO and LUMO parameters exert a significant influence on chemical reactions [52]. The HOMO represents the electron donating ability, while the LUMO signifies the electron accepting capability. In determining molecular electrical transport properties, the energy gap between the HOMO and LUMO (ΔE_{H-L}) operates as a significant parameter [53]. Furthermore, it has been demonstrated that the HOMO-LUMO gap primarily controls bond strength [54, 55]. The larger the bond dissociation energy of the HB, the smaller the ΔE_{H-L}. In both the APT and HET groups, electron-donating substitutions such as Ph, $PhOCH_3$, and $NHCH_3$ lead to an increase in the HOMO and LUMO energies; conversely, electron-withdrawing substitutions such as F, Cl, and NO_2 result in a decrease in energy. Additionally, the composition with $PhOCH_3$ substitution exhibits the highest reactivity because it possesses the lowest energy gap (refer to Table 7). The determination of chemical hardness (η) and electronic chemical potential (μ) for molecules is achieved through the utilization of Koopman's theorem [56] as presented below:

$$\eta = \frac{(E_{LUMO} - E_{HOMO})}{2} \quad (5)$$

$$\mu = \frac{(E_{LUMO} + E_{HOMO})}{2} \quad (6)$$

where E_{LUMO} is the energy of the lowest unoccupied molecular orbital and E_{HOMO} is the energy of the highest occupied molecular orbital. Chemical hardness, as defined by literature sources [57, 58], can be characterized as the degree of resistance exhibited by a given chemical species to alter its electronic configuration. Additionally, the electronic chemical potential provides insight into the tendency of an electron cloud to escape. Conversely, softness, which is the opposite of hardness, measures the ease of charge transfer.

Based on the findings presented in Table 7, it is evident that $PhOCH_3$ is the softest compound in both the APT and HET groups, while CH_2OCH_3 and F are identified as the hardest, respectively. A thorough examination of Table 7 also indicates that the chemical potential values increase for electron-donating substituents, whereas they decrease for electron-withdrawing ones. Notably, the NO_2 substitution exhibits the lowest chemical potential, whereas the $PhOCH_3$ substitution corresponds to the highest amount. The HOMO and LUMO orbitals for APT and its F and Ph derivatives are illustrated in Scheme 10. The HOMO of APT depicts an antibonding character at C=S and C–N bonds, and there is no electronic projection over the phenyl ring and H and F atoms. Meanwhile, the LUMO displays a larger electronic projection over the N–H and C–C bonds among the analyzed systems.

3.9. Water and CCl_4 solutions

The effect of the solvent on the HB energy is evaluated in this study by employing the PCM method as described in reference [28]. It is important to note that the PCM approach does not incorporate the explicit presence of solvent molecules but rather is based solely on the mutual electrostatic polarities of the solute and solvent. Two solvents with distinct polarities are selected for analysis. These solvents, water and CCl_4, exhibit dielectric constants of 80.0 and 2.3, respectively. The disparity in the calculated results between the gas phase and solution can be attributed to the polarity of the substituents, intramolecular interactions within the structures under investigation, and the solvent environment. The outcomes of the study indicate that the relative stability of the studied molecules reduces with an increment in the dielectric constant of the solvent (Table S1 of the supplementary material). As a result, the least stable structures are observed in the water.

The structural parameters determined thro

the employed solutions have been documented in Table S1. Our research reveals that the parameters relating to HB energy, such as the N-H bond length and H···S distance, undergo significant changes when solvent influence is considered. For the studied compounds, the N-H bond length experiences a reduction from the gas

phase to CCl_4 and subsequently to water (excluding F in HET), while the H···S distance increases. This indicates a decrease in HB strength in the solution phase compared to the gas phase. In the solution phase, systems with Ph substitution are found to be the strongest, while those with F substitution are the weakest, similar to the gas phase. The topological parameters are significantly altered by the solvent effect. Table S1 demonstrates that the parameters determining the strength of the HB, specifically, $\rho_{H\cdots S}$ and $\nabla^2\rho_{H\cdots S}$, decrease from the gas phase to CCl_4 and then to water. These findings confirm that the interaction in the solution phase is weaker than that in the gas phase.

The dipole moment is a crucial factor in determining the stability of molecules in a specific phase, and its assessment provides valuable insights. The presence of non-zero dipole moment signifies the molecule's polarity, which expounds on the movement of electric charge within the molecule [59]. Moreover, the direction of the dipole moment vector in a molecule is directly related to the positive and negative charge centers [60]. Table S2 presents the calculated dipole moments (μ°) in both the gas phase and solution. The results indicate an increment in dipole moment with an increase in the solvent's dielectric constant. The highest dipole moment is observed in water and the lowest value is in the gas phase. Among all phases, the APT and HET groups exhibit the highest and lowest dipole moments, respectively. Additionally, the NO_2 substitution results in the largest dipole moment within the gas phase and CCl_4, while the smallest dipole moment is associated with the OH substitution.

Table 7. The energy values of HOMO and LUMO (E_{HOMO} and E_{LUMO}) and their energy gap ($\Delta E_{H\text{-}L}$), chemical hardness (η) and electronic chemical potential (μ) in terms of eV.

	APT					**HET**				
	E_{HOMO}	E_{LUMO}	$\Delta E_{H\text{-}L}$	η	μ	E_{HOMO}	E_{LUMO}	$\Delta E_{H\text{-}L}$	η	μ
H	-0.218	-0.082	0.136	0.068	-0.150	-0.234	-0.110	0.124	0.062	-0.172
CH_2OCH_3	-0.217	-0.080	0.137	0.069	-0.149	-0.231	-0.106	0.125	0.062	-0.168
Cl	-0.232	-0.096	0.136	0.068	-0.164	-0.250	-0.124	0.126	0.063	-0.187
F	-0.231	-0.096	0.135	0.067	-0.163	-0.251	-0.124	0.127	0.063	-0.188
$NHCH_3$	-0.215	-0.081	0.135	0.067	-0.148	-0.220	-0.107	0.113	0.057	-0.163
NO_2	-0.248	-0.111	0.137	0.068	-0.179	-0.261	-0.138	0.122	0.061	-0.200
OH	-0.219	-0.088	0.131	0.065	-0.153	-0.234	-0.116	0.118	0.059	-0.175
Ph	-0.219	-0.084	0.136	0.068	-0.151	-0.231	-0.110	0.121	0.061	-0.171
$PhOCH_3$	-0.210	-0.081	0.129	0.065	-0.146	-0.217	-0.107	0.110	0.055	-0.162
SH	-0.227	-0.091	0.136	0.068	-0.159	-0.241	-0.118	0.124	0.062	-0.180

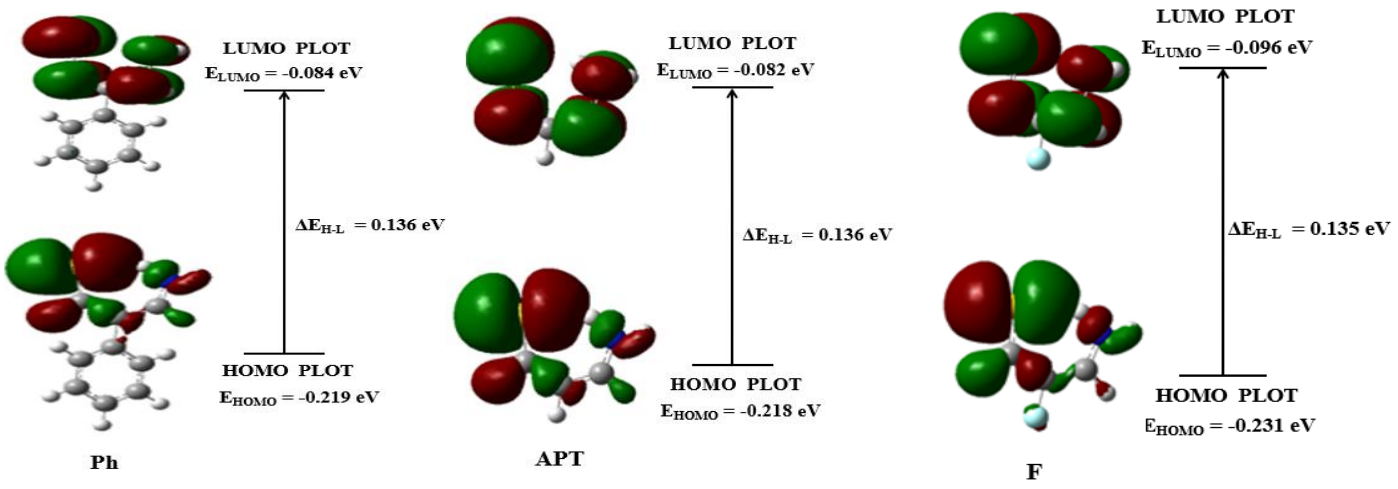

Scheme 10. The HOMO and LUMO orbitals for APT and its F and Ph derivatives.

4. Conclusions

This investigation considers the influence of substitution on the HB energies of N-H···S intramolecular bridges in the APT and HET groups employing the B3LYP/6-311++G(d,p) computational level. Both gas phase and solution data are scrutinized. The outcomes of DFT calculations reveal that HB formation can cause elongation of the N-H bond and shortening of the H···S distance. Moreover, quantum mechanical studies demonstrate that HB formation leads to shifts in the N-H stretching frequencies towards lower values. Based on the collected data, the HB strength of the HET group and its derivatives is higher than that of the APT. In other words, replacing the carbon atom with nitrogen within the structure increases the HB energy. In the evaluation of all substituents, electron-donating groups, such as Ph, strengthen the HB, whereas electron-withdrawing groups, such as F, weaken it. The findings derived from AIM calculations illustrate that the strength of the HB is heightened with an increase in the $\rho_{H\cdots S}$ value. For all investigated compounds, it is observed that the H···S bond exhibits low ρ, $\nabla^2\rho > 0$, $H_C > 0$, and $-G_C/V_C > 1$. These attributes are characteristic of closed-shell interactions and signify the electrostatic nature of the H···S bonding. The NBO approach is employed to compute the interaction between the LP_S and the σ^*_{N-H}, which revealed that the largest interaction is related to the strongest HB.

An additional methodology employed to examine HBs is the utilization of NMR. The strengthening of the HB leads to a displacement of the ^1H chemical shift towards the lower fields. The obtained outcomes reveal that in both the APT and HET groups, the Ph substitution, which has the strongest HB, is associated with the highest chemical shift value. The evaluation of the aromaticity of the HB pseudo-ring is conducted by applying different indices such as HOMA, FLU, NICS, PDI, and ATI, and the correlation between these indices with substitution constants is scrutinized. The findings reveal that the PDI index displays the most substantial correlations with σ^- and R^- in both the APT and HET groups. In the molecular orbital analysis of the APT and HET compounds, $PhOCH_3$ exhibits the softest attributes, while CH_2OCH_3 and F exhibit the hardest, respectively. Additionally, the NO_2 substitution demonstrates the lowest chemical potential, whereas the $PhOCH_3$ substitution corresponds to the highest amount. To investigate the effect of the environment on the strength of HBs, the calculations are conducted in two solvents, namely water and CCl_4. The outcomes indicate that HB strength is lower in the solution as compared to the gas phase. A noteworthy correlation is observed between the HB energy and the various parameters such as geometrical, topological, frequency, NMR data, and second-order perturbation energy, thus implying that these parameters are instrumental in assessing the HB strength.

The future scope of the present work includes some potential areas of interest and applications for this type of research such as: **Understanding molecular interactions:** The study of hydrogen bonding, charge transfer, and resonance in organic compounds can contribute to a better understanding of molecular interactions and their effects on the properties and behavior of these compounds. **Designing new materials:** Insights gained from these investigations can be applied to the design and synthesis of new materials with desired properties, such as improved conductivity,

catalytic activity, or optical properties. **Catalysis:** This analysis can be applied to the design of more efficient catalysts for various chemical reactions, including those involved in the conversion of epoxides. **Corrosion resistance:** This exploration can help in the development of corrosion-resistant alloys and coatings. **Drug design:** This study can contribute to the design of new drugs that target specific molecular interactions, such as the post-synaptic action of excitatory amino acids.

Acknowledgements

The authors wish to thank Payame Noor University, Tehran, Iran, for its support.

Supplementary data

Supplementary data to this article can be found online at doi:

References

[1] G.A. Jeffrey, W. Saenger, Hydrogen Bonding in Biological Structures, Springer, Berlin (1991).

[2] S. Scheiner, Hydrogen bonding, Oxford University Press, New York (1997).

[3] G.R. Desiraju, T. Steiner, The Weak Hydrogen Bond in Structural Chemistry and Biology, Oxford University Press, New York (1999).

[4] A.D. Buckingham, J.E. Del Bene, S.A.C. McDowell, The hydrogen bond. *Chem. Phys. Lett.*, 463 (2008) 1–10.

[5] P. Hobza, Z. Havlas, Blue-Shifting Hydrogen Bonds. *Chem. Rev.*, 100 (2000) 4253–4264.

[6] M. Mohammadi, F. Alirezapour, A. Khanmohammadi, DFT calculation of the interplay effects between cation–π and intramolecular hydrogen bond interactions of mesalazine drug with selected transition metal ions (Mn^{+}, Fe^{2+}, Co^{+}, Ni^{2+}, Cu^{+}, Zn^{2+}). *Theor. Chem. Acc.*, 140 (2021) 104.

[7] M. Cuma, S. Scheiner, T. Kar, Competition between rotamerization and proton transfer in o-hydroxybenzaldehyde. *J. Am. Chem. Soc.*, 120 (1998) 10497–10503.

[8] M. Mohammadi, A. Khanmohammadi, Theoretical investigation on the non-covalent interactions of acetaminophen complex in different solvents: study of the enhancing effect of the cation–π interaction on the intramolecular hydrogen bond. *Theor. Chem. Acc.*, 139 (2020) 141.

[9] F. Alirezapour, A. Khanmohammadi, Computational study of noncovalent interactions within the various complexes of para aminosalicylic acid and Cr^{2+}, Mn^{+}, Fe^{2+}, Co^{+}, Ni^{2+}, Cu^{+}, Zn^{2+} cations: exploration of the enhancing effect of the cation–π interaction on the intramolecular hydrogen bond. *Theor. Chem. Acc.*, 139 (2020) 180.

[10] E. Abdulkareem Mahmood, M.R. Poor Heravi, A. Khanmohammadi, S. Mohammadi Aghdam, A.G. Ebadi, S. Habibzadeh, DFT calculations, structural analysis, solvent effects, and non-covalent interaction study on the para-aminosalicylic acid complex as a tuberculosis drug: AIM, NBO, and NMR analyses. *J. Mol. Model.*, 28 (2022) 297.

[11] M. Mohammadi, F. Hoseinpour, A. Khanmohammadi, A DFT theoretical investigation on the interplay effects between cation-π and intramolecular hydrogen bond interactions in the mesalazine···Fe^{2+} binary complex. *Theor. Chem. Acc.*, 141 (2022) 38.

[12] M. Pirgheibi, M. Mohammadi, A. Khanmohammadi, A comparative study of interplay effects between the cation-π and intramolecular hydrogen bond interactions in the various complexes of methyl salicylate with Mn^{+}, Fe^{2+}, Co^{+}, Ni^{2+}, Cu^{+}, and Zn^{2+} cations. *Struct. Chem.*, 32 (2021) 1529–1539.

[13] M. Pirgheibi, M. Mohammadi, A. Khanmohammadi, Density functional theory study of the interplay between cation–π and intramolecular hydrogen bonding interactions in complexes involving methyl salicylate with Li^{+}, Na^{+}, K^{+}, Be^{2+}, Mg^{2+}, Ca^{2+} cations. *Comp. Theor. Chem.*, 1198 (2021) 113172.

[14] A. Khanmohammadi, M. Mohammadi, Theoretical study of various solvents effect on 5-fluorouracil-vitamin B3 complex using PCM method. *J. Chil. Chem. Soc.*, 64 (2019) 4265-4272.

[15] F. Ravari, A. Khanmohammadi, Interaction of the vitamin B3 with the parent uracil and anticancer uracil's: a detailed computational approach. *Org. Chem. Res.*, 6 (2019) 36-53.

[16] L. Hokmabadi, A. Khanmohammadi, Theoretical study on the interaction between 5-fluorouracil anticancer drug and nitrosamine as a family of potent carcinogenic compounds in different solvents: a quantum chemical study. *Org. Chem. Res.*, 6 (2020) 242-256.

[17] L. Guadagno, M. Raimondo, C. Naddeo, L. Vertuccio, S. Russo, G. Iannuzzo, E. Calabrese, Rheological, thermal and mechanical characterization of toughened self-healing supramolecular resins, based on hydrogen bonding. *Nanomaterials*, 12 (2022) 4322.

[18] X. Ran, Y. Wang, J. Lu, R. Sun, J.-B. Xu, N. Yang, H. Yin, C.-P. Wong, Effect of hydrogen bonds on the thermal transport in a precisely branched polyethylene with ordered and amorphous structures. *Comput. Mater. Sci.*, 205 (2022) 111191.

[19] R.A. Berenguer, N.B. Lima, V.M.E. Lima, A.M.L. Estolano, Y.V. Póvoas, N.B.D. Lima, The role of hydrogen bonds on the mechanical properties of cement-based mortars applied to concrete surfaces. *Cem. Concr. Compos.*, 115 (2021) 103848.

[20] H. Bi, X. Wang, H. Liu, Y. He, W. Wang, W. Deng, X. Ma, Y. Wang, W. Rao, Y. Chai, H. Ma, R. Li, J. Chen, Y. Wang, M. Xue, A universal approach to aqueous energy storage via ultralow-cost electrolyte with super-concentrated sugar as hydrogen-bond-regulated solute. *Nat. Commun.*, 32 (2020) 2000074.

[21] G. Liu, J. Xie, S. Wang, Q. Wang, S. Gao, Y. Yuan, J. Lu, Hydrogen-bonding reinforced flexible composite electrodes for enhanced energy storage. *Nat. Commun.*, 32 (2022) 2108003.

[22] M.M. Mirhosseini, R. Khordad, B. Vaseghi, Effect of hydrogen bonding on drug loading using a nanographene surface: A molecular dynamics study. *Chin. J. Phys.*, 62 (2019) 99-105.
[23] X. Duan, H. Chen, C. Guo, Polymeric Nanofibers for Drug Delivery Applications: A Recent Review. *J. Mater. Sci. Mater. Med.*, 33 (2022) 78.
[24] M.S.M. Serafim, S.N. Lavorato, T. Kronenberger, Y.V. Sousa, G.P. Oliveira, S.G. dos Santos, E.G. Kroon, V.G. Maltarollo, R.J. Alves, B.E.F. Mota, Antibacterial activity of synthetic 1,3-bis(aryloxy)propan-2-amines against Gram-positive bacteria. *MicrobiologyOpen.*, 8 (2019) e814.
[25] P.S. Leung, The physiology of a local renin–angiotensin system in the pancreas. *J. Physiol.*, 580 (2007) 31–37.
[26] M. Weerawatanakorn, J.-C. Wu, M.-H. Pan, C.-T. Ho, Reactivity and stability of selected flavor compounds. *J. Food Drug Anal.*, 23 (2015) 176-190.
[27] M.J. Frisch, G.W. Trucks, H.B. Schlegel, G.E. Scuseria, M.A. Robb, J.R. Cheese-man, G. Scalmani, V. Barone, B. Mennucci, G.A. Petersson, H. Nakatsuji, M. Caricato, X. Li, H.P. Hratchian, A.F. Izmaylov, J. Bloino, G. Zheng, J.L. Son-nenberg, M. Hada, M. Ehara, K. Toyota, R. Fukuda, J. Hasegawa, M. Ishida, T. Nakajima, Y. Honda, O. Kitao, H. Nakai, T. Vreven, J.A. Montgomery Jr, J.E. Peralta, F. Ogliaro, M.J. Bearpark, J. Heyd, E.N. Brothers, K.N. Kudin, V.N. Staroverov, R. Kobayashi, J. Normand, K. Raghavachari, A.P. Rendell, J.C. Bu-rant, S.S. Iyengar, J. Tomasi, M. Cossi, N. Rega, N.J. Millam, M. Klene, J.E. Knox, J.B. Cross, V. Bakken, C. Adamo, J. Jaramillo, R. Gomperts, R.E. Stratmann, O. Yazyev, A.J. Austin, R. Cammi, C. Pomelli, J.W. Ochterski, R.L. Martin, K. Morokuma, V.G. Zakrzewski, G.A. Voth, P. Salvador, J.J. Dannenberg, S. Dapprich, A.D. Daniels, Ö. Farkas, J.B. Foresman, J.V. Ortiz, J. Cioslowski, D.J. Fox, Gaussian 09, Gaussian, Inc., Wallingford, CT, USA (2009).
[28] J. Tomasi, R. Cammi, B. Mennucci, C. Cappelli, S. Corni, Quantum mechanical continuum solvation models. *Phys. Chem. Chem. Phys.*, 4 (2002) 5697-5709.
[29] R.F.W. Bader, Atoms in molecules: a quantum theory, Clarendon Press, Oxford (1990).
[30] F.W. Biegler-König, R.F.W. Bader, Y.H. Tang, Y. Tal, Chemical bonding: the electron-density distribution of some molecules and ions determined from topological analysis of Compton-profile parameters. *J. Comput. Chem.*, 3 (1982) 317-333.
[31] F. Biegler Konig, J. Schonbohm, Update of the AIM2000-program for atoms in molecules. *J. Comput. Chem.*, 23 (2002) 1489-1494.
[32] E. Espinosa, E. Molins, Retrieving interaction potentials from the topology of the electron density distribution: the case of hydrogen bonds. *J. Chem. Phys.*, 113 (2000) 5686–5694.
[33] A.E. Reed, L.A. Curtiss, F. Weinhold, Intermolecular interactions from a natural bond orbital, donor-acceptor viewpoint. *Chem. Rev.*, 88 (1988) 899-926.
[34] P. Pulay, J.F. Hinton, K. Wolinski, In: J.A. Tossel (ed), Nuclear magnetic shieldings and molecular structure, Kluwer, Dordrecht (1993).
[35] W.J. Hehre, L. Radom, P.R. Schleyer, J.A. Pople, Ab initio molecular orbital theory, Wiley, New York (1986).
[36] T.M. Krygowski, M.K. Cyran˜ski, Crystal and molecular structure of 2,3-dihydro-1,5-benzothiazepine-4(5H)-one. *Tetrahedron*, 52 (1996) 1713-1722.
[37] J. Kruszewski, T.M. Krygowski, Crystal structure of 2-methyl-6-nitroaniline. *Tetrahedron Lett.*, 13 (1972) 3839-3842.
[38] T.M. Krygowski, Crystallographic studies of intermolecular interactions and their significance for structure-property relations. *J. Chem. Inf. Comput. Sci.*, 33 (1993) 70-78.
[39] M.K. Cyran´ski, T.M. Krygowski, A.R. Katritzky, P.v.R. Schleyer, To what extent can aromaticity be defined uniquely? *J. Org. Chem.*, 67 (2002) 1333-1338.
[40] J. Poater, X. Fradera, M. Duran, M. Solà, Are π-holes good or bad halogen bonding sites? *Chem. Eur. J.*, 9 (2003) 400-406.
[41] P. Bultinck, R. Ponec, S. Van Damme, Electrostatic potential, atomic charges, and chemical bonding. *J. Phys. Org. Chem.*, 18 (2005) 706-718.
[42] E. Matito, M. Duran, M. Solà, Quantum chemical topology study of the electron density and the Laplacian of the electron density in aromaticity and antiaromaticity. *J. Chem. Phys.*, 125 (2005) 059901.
[43] L.N. Kurkovskaya, N.N. Shapet'ko, V.A. Kogan, O.A. Osipov, T.A. Zhuchenko, Interaction of molecules in crystals of diphenylethylene derivatives and the origin of the effect of aromaticity on the crystal structure of organic compounds. *Theor. Exp. Chem.*, 9 (1975) 203-208.
[44] U. Koch, P.L.A. Popelier, Characterization of C-H-O hydrogen bonds on the basis of the charge density. *J. Phys. Chem.*, 99 (1995) 9747-9754.
[45] P. Popelier, Atoms in molecules. an Introduction, Prentice-Hall pearson Education Limited, Englewood Cliffs, NJ (2000).
[46] H. Raissi, A.F. Jalbout, M.A. Nasseri, M. Yoosefian, H. Ghassi, A. Hameed, Conformational analysis of 6-fluoro-4-arylquinazolines: A comparative study using DFT and ab initio methods. *Int. J. Quant. Chem.*, 108 (2008) 1444-1454.
[47] R.D. Parra, J. Ohlssen, Computational study of the thermochemistry of the hydrogen abstraction reactions from phenol by hydroperoxyl radical and methyl radical. *J. Phys. Chem. A*, 112 (2008) 3492-3501.
[48] M. Ziółkowski, S.J. Grabowski, J. Leszczynski, Noncovalent π-π stacking interactions: a benchmark theoretical study of the S66 set. *J. Phys. Chem. A*, 110 (2006) 6514-6520.
[49] P.v.R. Schleyer, C. Maerker, A. Dransfeld, H. Jiao, N.J.R.E. Hommes, Nucleus-independent chemical shifts: a simple and efficient aromaticity probe. *J. Am. Chem. Soc.*, 118 (1996) 6317-6318.
[50] H. Raissi, A. Khanmohammadi, F. Mollania, A theoretical DFT study on the structural parameters and intramolecular

hydrogen-bond strength in substituted (Z)-N-(Thionitrosomethylene) - thiohydroxylamine systems. *Bull. Chem. Soc. Jpn.*, 86 (2013) 1261-1271.
[51] C. Hansch, A. Leo, R.W. Taft, Linear substituent constants for correlation analysis in chemistry and biology. *Chem. Rev.*, 91 (1991) 165-195.
[52] K. Fukui, The path of chemical reactions - the IRC approach. *Sci.*, 217 (1982) 747-753.
[53] J.N. Liu, Z.R. Chen, S.F. Yuan, Study on the stability of DNA with different base compositions using scanning electrochemical microscopy. *J. Zhejiang. Univ. Sci. B*, 6 (2005) 584-589.
[54] H.Y. Liao, Synthesis of 2,3,4,5-tetra-substituted thiophenes via sequential cross-coupling reactions. *J. Chin. Chem. Soc.*, 56 (2009) 532-536.
[55] F.Y. Li, J.J. Zhao, A theoretical study of the reaction of Cl(2P) with H_2S. *J. At. Mol. Sci.*, 1 (2010) 68-72.
[56] T.A. Koopmans, Über die Zuordnung von Wellenfunktionen und Eigenwerten zu den einzelnen Elektronen eines atoms. *Physica.*, 1 (1934) 104-113.
[57] R.G. Pearson, Absolute electronegativity and absolute hardness of Lewis acids and bases. *J. Am. Chem. Soc.*, 107 (1985) 6801-6806.
[58] R.G. Parr, P.K. Chattaraj, Principle of maximum hardness. *J. Am. Chem. Soc.*, 113 (1991) 1854-1855.
[59] G. Buemi, F. Zuccarello, P. Vanalingam, M. Ramalingam, Ab initio study of tautomerism and hydrogen bonding of β–carbonylamine in the gas phase and in water solution. *Theor. Chem. Acc.*, 104 (2000) 226–234.
[60] M. Khalil, R.J. Woods, D.F. Weaver, V.H. Smith, An examination of intermolecular and intramolecular hydrogen bonding in biomolecules by AM1 and MNDO/M semiempirical molecular orbital studies. *J. Comput. Chem.*, 12 (1991) 584.